

RSC Advances



This is an *Accepted Manuscript*, which has been through the Royal Society of Chemistry peer review process and has been accepted for publication.

Accepted Manuscripts are published online shortly after acceptance, before technical editing, formatting and proof reading. Using this free service, authors can make their results available to the community, in citable form, before we publish the edited article. This *Accepted Manuscript* will be replaced by the edited, formatted and paginated article as soon as this is available.

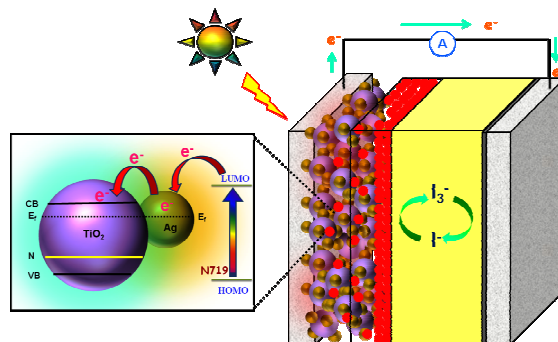
You can find more information about *Accepted Manuscripts* in the [Information for Authors](#).

Please note that technical editing may introduce minor changes to the text and/or graphics, which may alter content. The journal's standard [Terms & Conditions](#) and the [Ethical guidelines](#) still apply. In no event shall the Royal Society of Chemistry be held responsible for any errors or omissions in this *Accepted Manuscript* or any consequences arising from the use of any information it contains.

Enhanced Photovoltaic Performance of Silver@Titania Plasmonic Photoanode in Dye-Sensitized Solar Cells

Lim Su Pei, Alagarsamy Pandikumar, Huang Nay Ming, Lim Hong Ngee

Graphical Abstract



Ag@TiO₂ plasmonic photoanode modified dye-sensitized solar cells showed enhanced photovoltaic performance due to surface plasmon resonance effect.

Enhanced Photovoltaic Performance of Silver@Titania Plasmonic Photoanode in Dye-Sensitized Solar Cells

Lim Su Pei,¹ Alagarsamy Pandikumar,^{1*} Huang Nay Ming,^{1*} Lim Hong Ngee^{2,3*}

¹ Low Dimensional Materials Research Centre, Department of Physics, Faculty of Science, University of Malaya, 50603 Kuala Lumpur, Malaysia

² Department of Chemistry, Faculty of Science, Universiti Putra Malaysia, 43400 UPM Serdang, Selangor, Malaysia

³ Functional Device Laboratory, Institute of Advanced Technology, Universiti Putra Malaysia, 43400 UPM Serdang, Selangor, Malaysia

Corresponding author's: pandikumarinbox@gmail.com (Pandikumar A)
huangnayming@um.edu.my (Huang N.M.) and janet_limhn@yahoo.com (Lim H.N.)

Abstract

In the present investigation, silver@titania (Ag@TiO₂) plasmonic nanocomposite materials with different Ag content were prepared using a simple one-step chemical reduction method and used as a photoanode in high-performance dye-sensitized solar cells. Transmission electron microscopic images revealed the uniform distribution of ultra-small Ag nanoparticles with a particle size range of 2–4 nm on the TiO₂ surface. The incorporation of Ag on the TiO₂ surface significantly influenced the optical properties in the region of 400–500 nm because of the surface plasmon resonance effect. The dye-sensitized solar cells (DSSCs) assembled with the Ag@TiO₂-modified photoanode demonstrated an enhanced solar-to-electrical energy conversion efficiency (4.86 %) compared to that of bare TiO₂ (2.57 %), due to the plasmonic effect of Ag. In addition, the Ag nanoparticles acted as an electron sink, which retarded the charge recombination. The influence of the Ag content on the overall efficiency was also investigated, and the optimum Ag content with TiO₂ was found to be 2.5 wt.%. The enhanced solar energy conversion efficiency of the Ag@TiO₂ nanocomposite makes it a promising alternative to conventional photoanode-based DSSCs.

Keywords: Photoanode; Ag@TiO₂; Nanocomposite; Plasmonic effect; Solar Energy; Dye-Sensitized Solar Cells

1. Introduction

Renewable energy sources are the most important approaches and signify an important method for gaining independence from fossil fuels. Utilizing solar energy is certainly one of the most viable ways to solve the world's energy crisis. Dye-sensitized solar cells (DSSCs) have emerged as promising candidates for harnessing solar power because of their low cost, flexibility, ease of production, relatively high energy conversion efficiency, and low toxicity to the environment.¹ Since first being introduced by Gratzel and co-workers in 1991, many strategies have been employed to achieve high-performance DSSCs, including novel counter electrodes, electrolytes, dyes, and semiconductor photoanode materials. Among these, the photoanode plays a crucial role in determining the cell performance. So far, titanium dioxide (TiO₂)-based material is one of the most promising materials for a DSSC due to its low cost, abundance, nontoxicity, safety, large surface area for maximum dye uptake and matched energy and band structure.^{2,3} However, the major drawback associated with the use of TiO₂ is its random electron transport, which will cause the electron-hole recombination process and hence affect the overall performance.^{4,5}

There is an active search to overcome the deficiency of TiO₂-based DSSCs such as through surface modification with metal nanoparticles, doping of metals and non-metals, semiconductor coupling, and hybridizing with a carbon materials.⁶⁻⁹ In the present decade, surface of TiO₂ has been modified with noble metal nanoparticles such as silver (Ag), with the aim of improving the efficiency of a DSSC. The Ag nanoparticles play dual roles in the DSSC performance, including the enhancement of the absorption coefficient of the dye and optical absorption due to surface plasmonic resonance.¹⁰⁻¹² Moreover, they act as an electron sink for photoinduced charge carriers, improve the interfacial charge transfer process, and minimize the charge recombination, thereby enhancing the electron transfer process in a

DSSC.¹³⁻¹⁵ Hence, the performance of a DSSC with Ag@TiO₂ plasmonic nanocomposite material-modified photoanodes has been actively investigated.¹³⁻¹⁵

To make use of economically viable Ag to boost the DSSC performance, it is essential to control both the size and distribution of the nanoparticles on the TiO₂ surface. Two methods are commonly employed for Ag-TiO₂ nanocomposite preparation: (i) a two-step method involving the chemical and physical adsorption of preformed Ag nanoparticles on the TiO₂ surface¹⁶⁻¹⁸ and (ii) the photoreduction of Ag on the TiO₂ surface.^{19,20} However, these synthetic methods are ineffective because of the aggregation of Ag nanoparticles in the first method and the difficulty controlling the size of the Ag nanoparticles in the later one.

In the present study, we successfully developed a facile synthesis method to prepare uniformly distributed Ag nanoparticles deposited on TiO₂ using a simple one-step chemical reduction method without adding any stabilizer or surfactant for DSSC application. The as-prepared Ag@TiO₂ plasmonic nanocomposites were characterized using various suitable analytical techniques and used as photoanodes in the DSSCs. The Ag@TiO₂ plasmonic nanocomposite-modified photoanode showed an enhanced solar energy conversion efficiency compared to that of a bare TiO₂-based DSSC. The effect of the Ag content on the DSSC performance was also investigated. There are many positive aspects of the Ag-modified TiO₂, including the synergetic interaction of the Ag nanoparticles on the TiO₂ surface, surface plasmon resonance effect, reduction of the band gap, and enhancement of the charge transfer process. These multifunctional properties of the prepared Ag@TiO₂ plasmonic nanocomposite will lead to superior performance in a DSSC.

2. Experimental Methods

2.1. Materials and characterization techniques

Titanium dioxide (P25) was purchased from Acros Organics. Silver nitrate (AgNO_3) and sodium borohydride (NaBH_4) were purchased from Merck. Indium tin oxide (ITO) conducting glass slides ($7 \Omega/\text{sq}$) were purchased from Xin Yan Technology Limited, China. The N719 (Ruthenizer 535-bisTBA) dye and Iodolyte Z-100 were received from Solaronix. The crystalline phase of the samples was studied via X-ray diffraction (XRD; D5000, Siemens), using copper $K\alpha$ radiation ($\lambda = 1.5418 \text{ \AA}$). The morphologies of the prepared samples were examined using a Hitachi-SU 8000 field emission scanning electron microscope and JEOL JEM-2100 F high-resolution transmission electron microscope. The absorption spectra were assessed using a Thermo Scientific Evolution 300 UV-vis absorption spectrophotometer. Photoluminescence and Raman spectra were collected using a Renishaw inVia 2000 system with an argon ion laser emitting at 325 and 532 nm, respectively. X-ray photoelectron spectroscopy (XPS) measurements were performed using synchrotron radiation from beamline no. 3.2 at the Synchrotron Light Research Institute, Thailand.

2.2. Synthesis of Ag@TiO_2 nanocomposite materials

The Ag@TiO_2 nanocomposite materials were prepared using a simple one-step chemical reduction method. Briefly, 500 mg of TiO_2 were added to aqueous solutions that contained different amounts of AgNO_3 (1, 2.5, 5, 10, and 20 wt %). Each mixture was vigorously stirred for 30 min at room temperature. The reduction of Ag^+ was carried out by the drop-wise addition of NaBH_4 until the color changed to greenish yellow. The appearance of this greenish yellow color indicated the formation of the Ag@TiO_2 nanocomposite, and the solution was continually stirred for another 30 min. The Ag@TiO_2 nanocomposite was collected and washed with distilled water and ethanol several times by centrifugation. Finally, the product was dried in an oven at $60 \text{ }^\circ\text{C}$ and stored under a dark condition.

2.3. Fabrication of Ag@TiO₂-modified photoanode

Ag@TiO₂ modified photoanodes were fabricated using the following procedure. Initially, 300 mg of the Ag@TiO₂ nanocomposite was mixed in an ethanolic solution and stirred for 30 min. A 0.1 M quantity of TTIP was slowly introduced into the above reaction mixture and stirred until a homogenous solution was obtained. Finally, the Ag@TiO₂ nanocomposites were coated on a conducting side of the ITO using the doctor-blade technique with the aid of scotch-3M tape and the thickness of the film was ~12 μm. In order to obtain a stable photoanode, the film was dried at room temperature, sintered at 150 °C for 30 min in a muffle furnace, and then allowed to cool naturally to room temperature.

2.4. Fabrication of DSSCs and evaluation of their performances

The prepared Ag@TiO₂ plasmonic nanocomposite photoanodes were immersed in a ethanolic solution of 0.3 mM N719 (Ruthenizer 535-bisTBA) dye for 24 h at room temperature under a dark condition. The dye-adsorbed plasmonic photoanode was withdrawn from the solution and immediately but gently cleaned with ethanol. A platinum-sputtered ITO was placed on a dye-adsorbed photoanode, and they were clamped firmly together. A redox electrolyte (Iodolyte Z-100, Solaronix) solution was introduced into the cell assembly by capillary action. An active area of 0.5 cm² was used to measure the cell performance. A 150-W Xenon arc lamp (Newport, Model 69907) containing a simulated AM 1.5G filter with a manual shutter was used as a light source throughout the experiments. Prior to testing the photovoltaic parameter, an Avaspec-2048 fiber optic spectrophotometer was used to measure the light illumination intensity. The photocurrent signal measurements (J–V and J–T curves) and electrochemical properties of the fabricated DSSCs were studied by using a computer-controlled VersaSTAT 3 Electrochemical Workstation (Princeton Applied Research, USA).

3. Results and discussion

3.1. Optical properties of Ag@TiO₂ nanocomposite materials

In the present synthetic method, the formation of the Ag@TiO₂ nanocomposite takes place through the adsorption of Ag⁺ ions on the TiO₂ surface, followed by the chemical reduction of Ag⁺ by NaBH₄ at room temperature in the absence of any stabilizer and surfactant (**Fig. 1a**). The physical appearances of the Ag@TiO₂ with different quantities of Ag (wt %) are shown in **Fig. 1b**, shows that the nanocomposite becomes darker in color with increasing Ag content.

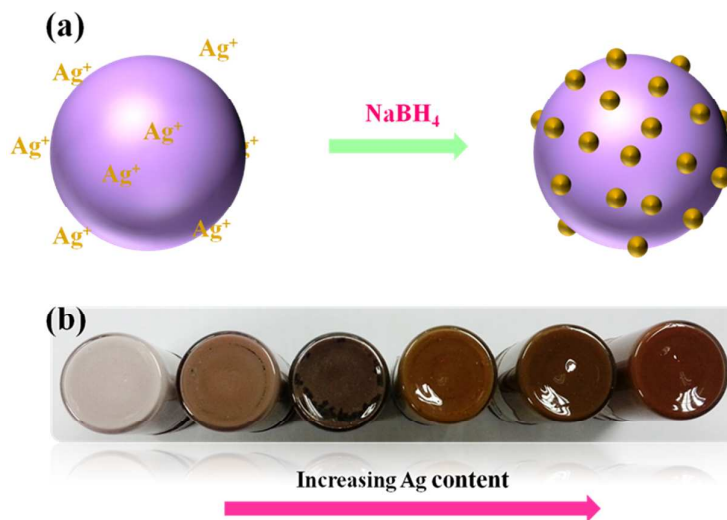


Fig. 1 (a) Schematic representation of formation of Ag on TiO₂ surface and (b) physical appearance of as-prepared Ag@TiO₂ nanocomposites with different Ag content.

The UV–vis absorption spectra of the TiO₂ and Ag@TiO₂ were recorded and are shown in **Fig. 2**. The TiO₂ did not show any absorbance in the visible region (**Fig. 2A**) because of the wide band gap (~3.2 eV). The deposition of Ag on the TiO₂ surface significantly influenced the absorption in the visible regions of 450 and 500 nm, which was due to the surface plasmon resonance (SPR) band of Ag nanoparticles.^{19, 21} A considerable shift in the adsorption edge toward the visible region was also observed for the Ag@TiO₂ sample. The

presence of Ag nanoparticles significantly influenced the visible light absorption properties of TiO₂. The band-gap energy (E_{bg}) of the prepared TiO₂ and Ag@TiO₂ were calculated using a well-known Tauc's plot method.^{22, 23} The relations of $(\alpha h\nu)^2$ versus $h\nu$ for the TiO₂ and Ag@TiO₂ are shown in **Fig. 2(B and C)**. It can be observed that the band-gap energy values of TiO₂ decreased from 3.36 eV to 3.22 eV with the addition of Ag nanoparticles. This may have been due to the presence of Ag, which decreased the absorbance band edge of TiO₂ close to the visible region.

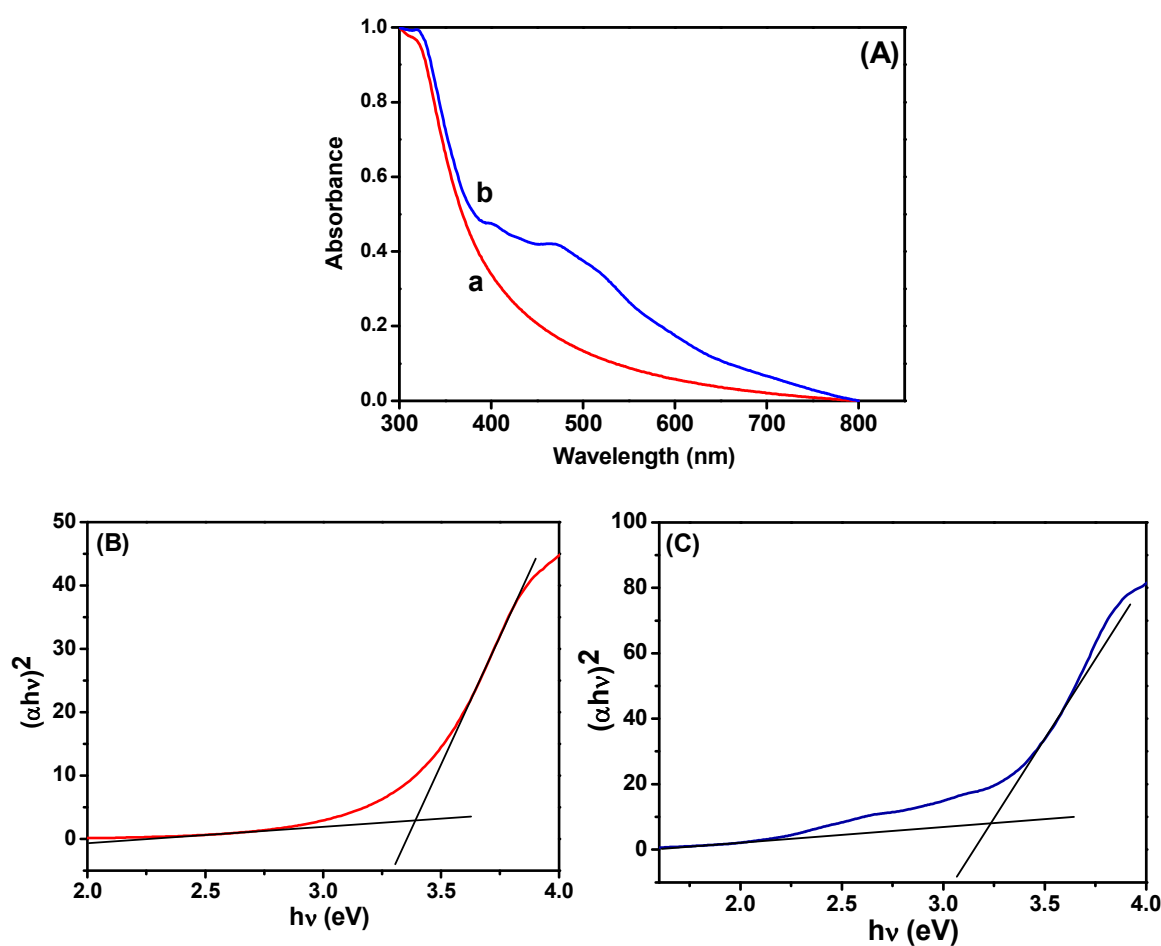


Fig. 2 (A) Absorption spectra of (a) TiO₂ and (b) Ag@TiO₂. Plots of $(\alpha h\nu)^2$ versus $h\nu$ obtained for (B) TiO₂ and (C) Ag@TiO₂.

Understanding the charge recombination process of a photoanode material is crucial because it can significantly influence the photovoltaic performance of a DSSC. The TiO₂ will

absorb incident photons with sufficient energy equal to or higher than the band-gap energy. This will produce photoinduced charge carriers ($h^+ \dots e^-$), and the recombination of photoinduced electrons and holes will release energy in the form of photoluminescence. Hence, a lower PL intensity indicates less charge recombination. The TiO_2 showed a broad and high PL intensity at around 580 nm due to the high photoinduced charge carrier recombination, whereas the PL intensity was minimized upon the addition of Ag on the TiO_2 surface (**Fig. 3(A)**). This was mainly attributed to the formation of the Schottky barrier at the Ag/ TiO_2 interface, which could act as an electron sink to efficiently prevent the electron-hole recombination process.²⁴ The Ag@ TiO_2 with 2.5 wt.% Ag showed the lowest PL emission intensity, which indicated the least electron-hole recombination compared to Ag contents of 1, 10, and 20 wt.% on the TiO_2 (**Fig. 3(B)**).

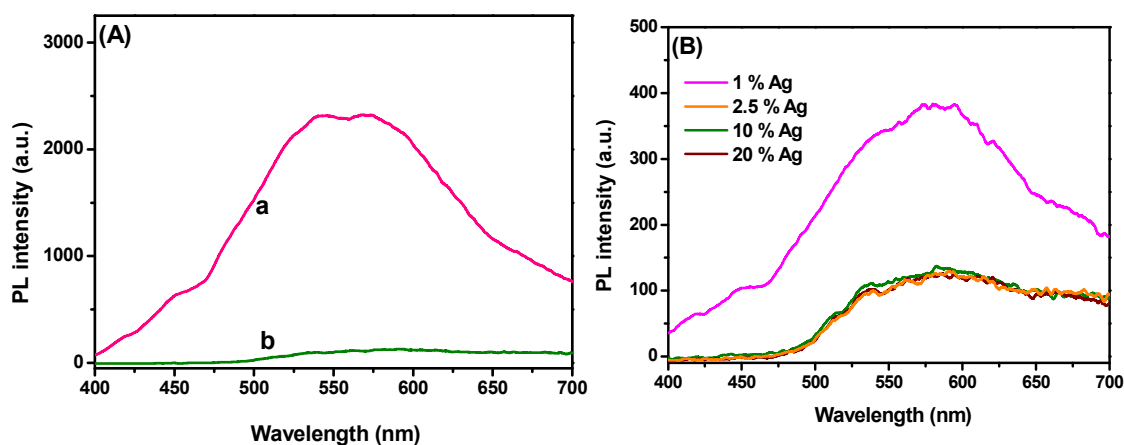


Fig. 3. (A) Photoluminescence spectra of (a) TiO_2 and (b) Ag@ TiO_2 nanocomposites under 325-nm laser excitation. (B) Photoluminescence spectra of Ag@ TiO_2 nanocomposites with different Ag contents under 325-nm laser excitation.

3.2. Crystalline properties of Ag@ TiO_2 nanocomposite materials

The X-ray diffraction patterns indicated that the TiO_2 and Ag@ TiO_2 were composed of mixed anatase and rutile phases (**Fig. 4**), which was in good agreement with the reference

patterns of JCPDS card Nos. 83-2243 and 21-1276, respectively. The diffraction peaks observed at the 2θ values of 25.42° , 38.68° , 48.15° , and 74.4° corresponded to the anatase phase of TiO_2 and were assigned to the (101), (004), (200), and (215) crystallographic planes, respectively. In contrast, the peaks at the 2θ values of 54.08° and 63.81° agreed well with the rutile phase of TiO_2 and were assigned to the (220) and (002) crystallographic planes, respectively. The crystallographic peaks due to the Ag overlapped with those for the rutile phase of the TiO_2 . Hence, the peaks were indistinguishable in Ag@TiO_2 .

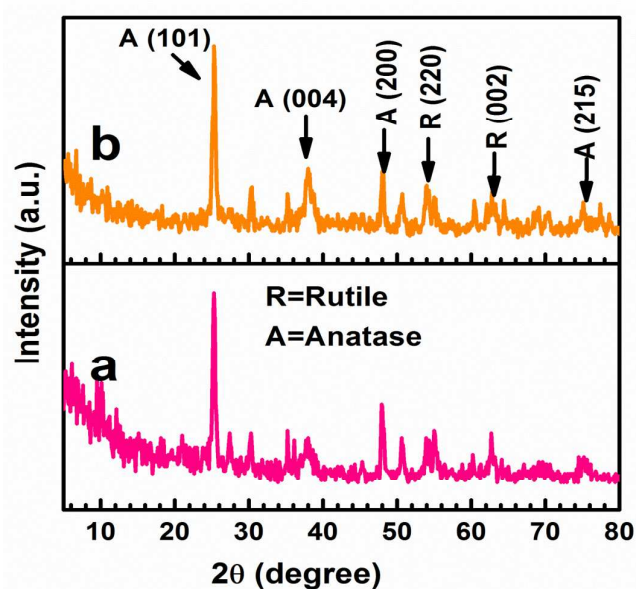


Fig. 4 X-ray diffraction patterns of (a) TiO_2 and (b) Ag@TiO_2 nanocomposites.

To further evaluate the phase identification of the TiO_2 and Ag@TiO_2 , Raman spectroscopy was performed in the range of $100\text{--}1000\text{ cm}^{-1}$, and the results are shown in **Fig. 5**. The anatase TiO_2 phase was observed at 153 , 198 , 396 , 516 , and 637 cm^{-1} , whereas the rutile TiO_2 phase was detected at 443 cm^{-1} .²⁵⁻²⁷ This clearly indicated that the TiO_2 and Ag@TiO_2 nanoparticles contained a mixture of anatase and rutile phases. No signals related to Ag particles were identified for the samples because of the relatively low concentration of Ag loaded onto the TiO_2 and its weak Raman scattering. An interesting observation is that the

peak intensities were reduced by the presence of Ag, but the position of the Raman signal remained the same and was broadened. This indicated that the interaction between the Ag and TiO₂ affected the Raman resonance of the TiO₂.²⁸ This observation showed the successful deposition of Ag on the TiO₂ surface without any phase transition.^{22, 27}

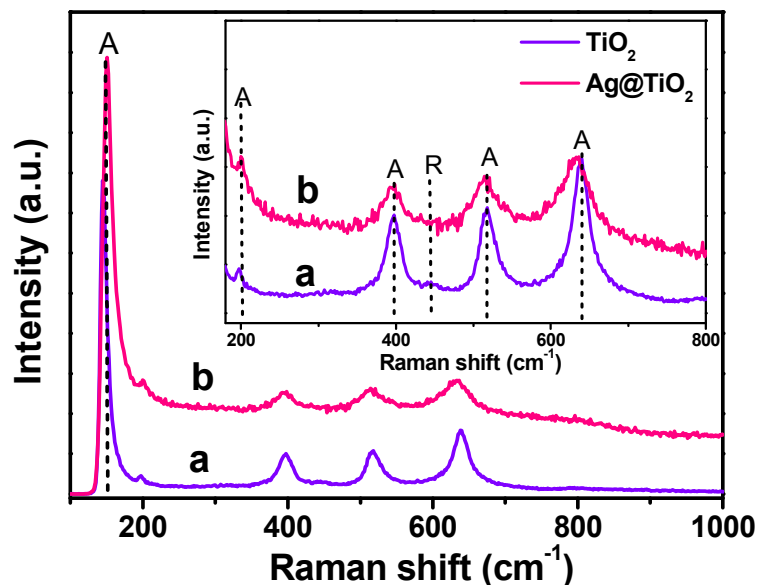


Fig. 5. Raman spectra of (a) TiO₂ and (b) Ag@TiO₂ nanocomposites with inset showing the anatase and rutile features of TiO₂.

3.3. XPS analysis of Ag@TiO₂ nanocomposite materials

The XPS spectra of the TiO₂ and Ag@TiO₂ were recorded to understand their chemical nature and are shown in **Fig. 6**. **Fig. 6A** shows the Ti 2p core level spectra for both samples, in which two peaks are observed at 454.1 and 459.9 eV corresponding to the binding energies of the Ti 2p_{3/2} and Ti 2p_{1/2} core levels due to the presence of the Ti(IV) state.²⁹ After the deposition of the Ag nanoparticles, it is obviously observed that the Ti 2p peak was shifted to lower binding energies due to its surrounding chemical environment.³⁰ **Fig. 6B** shows the O 1s spectra of the TiO₂ and Ag@TiO₂, and the binding energy of the O 1s state of the samples is located at 530.9 eV, which is assigned to the bulk oxides (O²⁻) in the

P25 lattice. The O 1s is slightly shifted to higher binding energies which indicate the increase in electron density around O atoms due to the interaction of residue precursor with TiO_2 .²¹ The binding energy found for the Ag $3d_{5/2}$ and Ag $3d_{3/2}$ levels are 367.5 and 373.5 eV, respectively (Fig. 6C), with a peak separation of 6 eV due to the metallic silver.²¹ The XPS analysis provided support for the existence of elements such as Ti, O, and Ag in the nanocomposite materials.

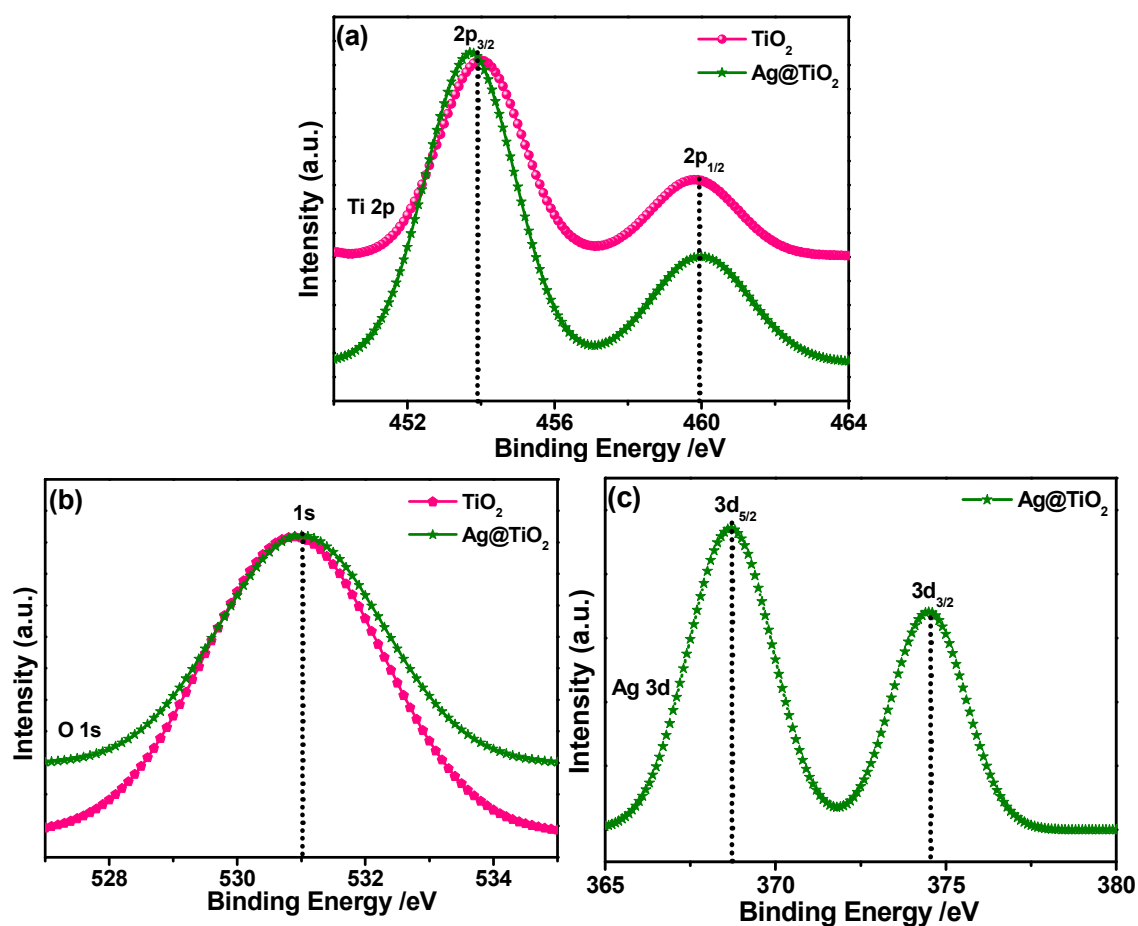


Fig. 6. XPS spectra of TiO_2 and Ag@TiO_2 and their corresponding (a) Ti 2p (b) O 1s, and (c) Ag 3d core-level spectra.

3.4. Morphological studies of Ag@TiO_2 nanocomposite materials

The microscopic morphologies of the as-prepared samples were studied using FESEM, TEM, and HRTEM. **Fig. S1a** shows the FESEM results for TiO_2 , which appear to be spherical with a uniform size. Upon the addition of Ag, no significant change in morphology was observed for the film (**Fig. S1b**).

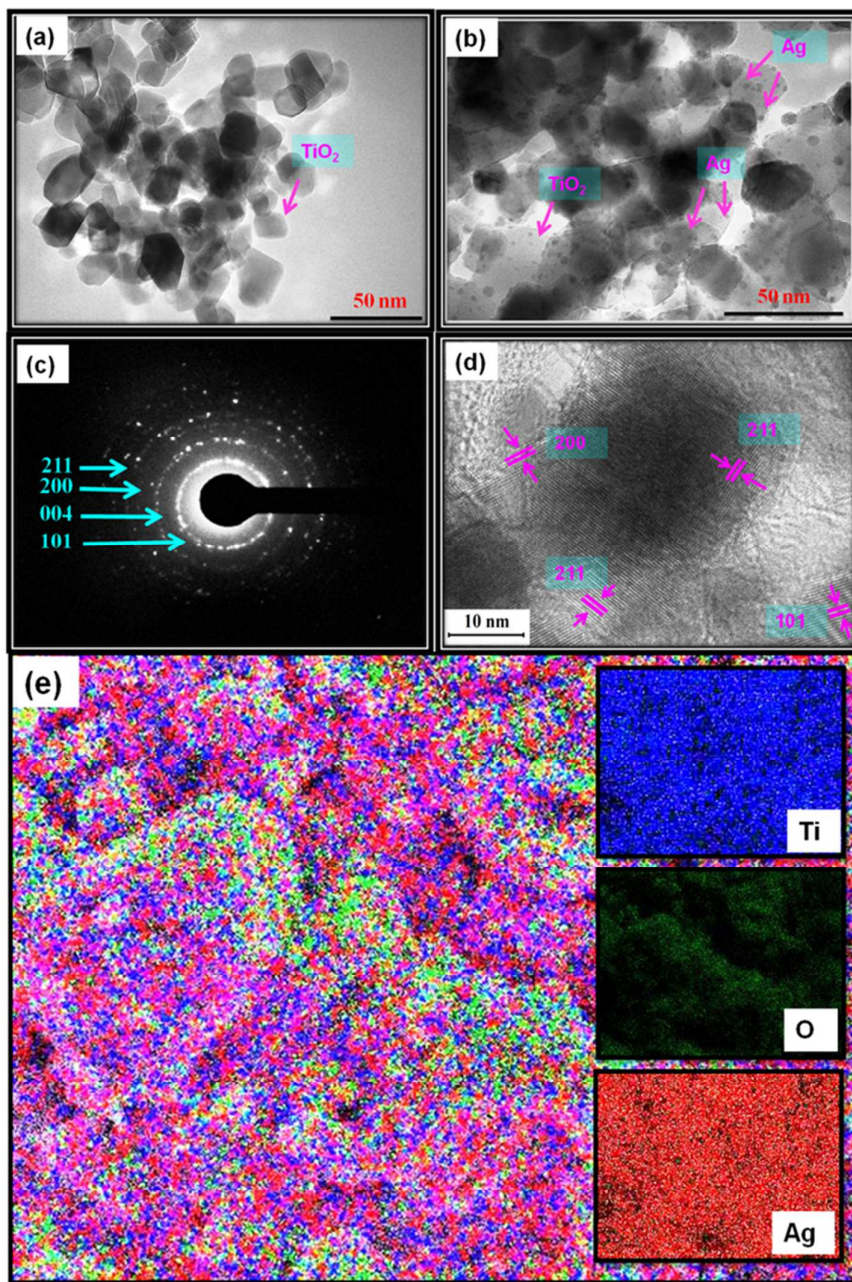


Fig. 7. TEM images of (a) TiO₂ and (b) Ag@TiO₂ nanocomposites, (c) SAED pattern, (d) lattice-resolved TEM image, and (e) elemental mapping of Ag@TiO₂ nanocomposite.

The EDX analysis results are shown in **Fig. S1c**, which shows Ti, O, C, and Ag. The C peak found in the EDAX spectrum is a result of carbon tape. Further, TEM images of TiO₂ and Ag@TiO₂ (2.5 wt% Ag) were also recorded and are shown in **Fig. 7(a and b)**, respectively. The TEM image shows that the Ag@TiO₂ nanoparticles are spherical in shape, with the TiO₂ particles having a size range of 20–25 nm. **Fig. 7b** clearly shows the deposition of distributed spherical and smaller Ag nanoparticles (2–4 nm) on the surface of TiO₂. **Fig. 7c** depicts the selected area electron diffraction (SAED) pattern of the nanocrystalline TiO₂ particles. This pattern clearly reveals bright concentric rings, which are due to the diffraction from the (211), (200), (004), and (101) planes of anatase TiO₂. The lattice resolved HRTEM image of the Ag@TiO₂ (**Fig. 7d**) shows d-spacing values for the lattice fringes of 2.28 Å and 2.50 Å, which correspond to the (200) and (101) rutile planes of TiO₂, respectively; whereas the interplanar spacing of 1.89 Å was assigned to the (200) plane of anatase TiO₂. In **Fig. 7e**, the areas of bright contrast on the element maps correlate with the Ti, O, and Ag signal maps.

3.5. Photovoltaic performances of Ag@TiO₂ plasmonic nanocomposite-modified photoanode-based DSSCs

The photovoltaic performances of the Ag@TiO₂ plasmonic nanocomposite-modified photoanode-based DSSCs with different Ag contents were evaluated under simulated solar AM 1.5G irradiation. Their obtained photocurrent density and photovoltage (J–V) curves are shown in **Fig. 8**, and their evaluated photovoltaic parameters are listed in **Table 1**. The Ag@TiO₂ plasmonic photoanode (2.5 wt.% of Ag) showed a higher efficiency (4.86 %) than the unmodified TiO₂ (2.57 %). The enhanced photovoltaic performance may have been due to

the plasmonic effect and rapid interfacial charge transfer that arose from the Ag nanoparticles on the TiO₂. The optimization of Ag on TiO₂ is essential from the economic and high-performance perspectives for a DSSC. Although increasing the Ag content on the TiO₂ surface beyond 2.5 wt.% showed a decrease in the conversion efficiency to 3.59 %, the observed results clearly revealed that the conversion efficiency of a DSSC was increased with an increase in the Ag content of the photoanode until it reached a maximum of 2.5 %. Then, a further increase in the Ag content eventually led to the decrease in conversion efficiency (**Fig. 8a and Table 1**). The decrease in the efficiency at high Ag loading is due to the free standing/excess Ag in the composite may oxidized to Ag(I)^{13, 31} and eroded by the electrolyte.¹³ The oxidation of the Ag will act as new recombination centre, thus reducing the number of the charge carrier led to decrease in the J_{sc} and V_{oc}. Consequently, the overall conversion efficiency of the DSSC would have deteriorated. Moreover, the addition of Ag more than 2.5 wt. % might result in decrease of the active surface area of TiO₂ interacted with the dye molecules. Hence, the recombination between the electrons and holes will increase leads to decrease of J_{sc} value. Consequently, the overall conversion efficiency of the DSSC would have deteriorated. The relationships between the photovoltaic parameters and Ag content on the TiO₂ surface are represented in **Fig. S2(a-c)** for better understanding.

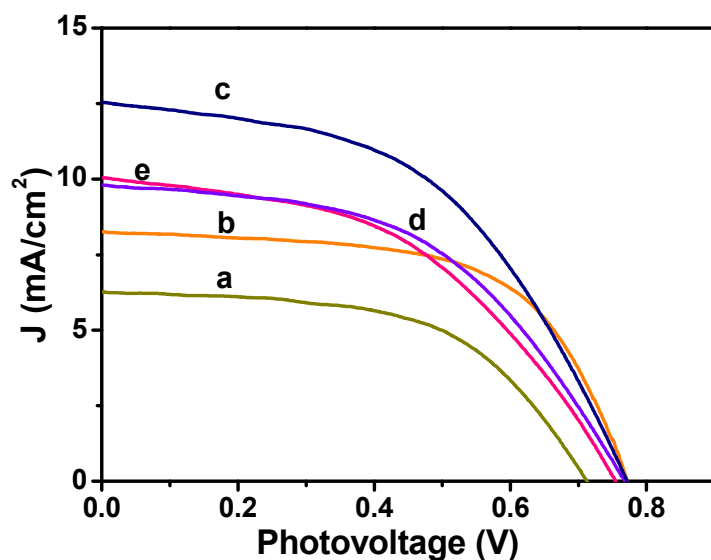


Fig. 8 Photocurrent density–photovoltage (J–V) curves obtained for Ag@TiO₂ nanocomposite thin films with (a) 0, (b) 1, (c) 2.5, (d) 10, and (e) 20 wt% of Ag content under 100 mW cm⁻² simulated AM 1.5G solar light irradiation.

Table 1. Photovoltaic parameters of Ag@TiO₂ nanocomposite-modified photoanode-based DSSCs with different Ag contents.

Ag (wt.%)	J_{sc} (mA/cm ²)	V_{oc} (V)	J_{max} (mA/cm ²)	V_{max} (V)	FF	η (%)
0	6.71	0.71	5.24	0.49	0.54	2.57
1	8.17	0.77	6.63	0.60	0.63	3.98
2.5	12.19	0.77	9.34	0.52	0.52	4.86
10	9.93	0.77	7.65	0.49	0.49	3.75
20	9.96	0.75	7.68	0.45	0.48	3.59

Footnote: The DSSC performance was evaluated under 100 mW cm⁻² simulated AM 1.5G solar light irradiation. J_{sc} : Short-circuit current density; V_{oc} : Open-circuit voltage; J_{max} : Maximum photocurrent density; V_{max} : Maximum photovoltage; FF: Fill factor; η : Power conversion efficiency. Area of the cell electrode was 0.5 cm².

3.6. Electrochemical behaviours of Ag@TiO₂ plasmonic photoanode-based DSSCs

In order to gain deeper insight into the interfacial charge transfer process within the fabricated DSSC, the electrochemical impedance spectra (EIS) were recorded in a frequency range between 0.01 Hz and 100 KHz, and are shown in **Fig. 9**. A well-defined semicircle in the middle-frequency region can be observed for the TiO₂ and Ag@TiO₂ based DSSCs. The intersection of a high-frequency semicircle at the real axis represents the equivalent series resistance of the device (R_s); the arc in the middle-frequency range between 1 and 1000 Hz represents the charge transfer resistance (R_{ct}) between the dye-adsorbed photoanode and the electrolyte interface.^{16, 18} From the Nyquist plot (**Fig. 9(A)**), the R_s values for the TiO₂ and Ag@TiO₂ nanocomposite-based DSSCs are 21.03 Ω and 23.96 Ω , respectively. The R_{ct} value

increased from 8.77Ω to 9.01Ω after the addition of the Ag. This increase in the R_{ct} value could affect the open-circuit voltage (V_{oc}) and fill factor (FF) of the DSSC device. Therefore, the origin of the higher J_{sc} in the Ag@TiO₂ is expected to arise from the device resistance (R_s) and charge transport dynamics determined by the electron lifetime (τ_n) and R_{ct} . Based on the Bode phase plots in **Fig. 9(B)**, the frequency was apparently shifted to a lower frequency region with the addition of Ag. The maximum frequencies (ω_{max}) in the middle-frequency region of the Bode plots for TiO₂ and Ag@TiO₂ were 2511.89 Hz and 1995.26 Hz, respectively. Because ω_{max} is inversely associated with the electron lifetime $\tau_n = 1/(2\pi f)$,^{32,33} a decrease in ω_{max} indicates a reduced rate for the charge-recombination process in the DSSC. Electrons with longer τ_n values will survive from the recombination. Therefore, it will be characterized by a larger R_{ct} .

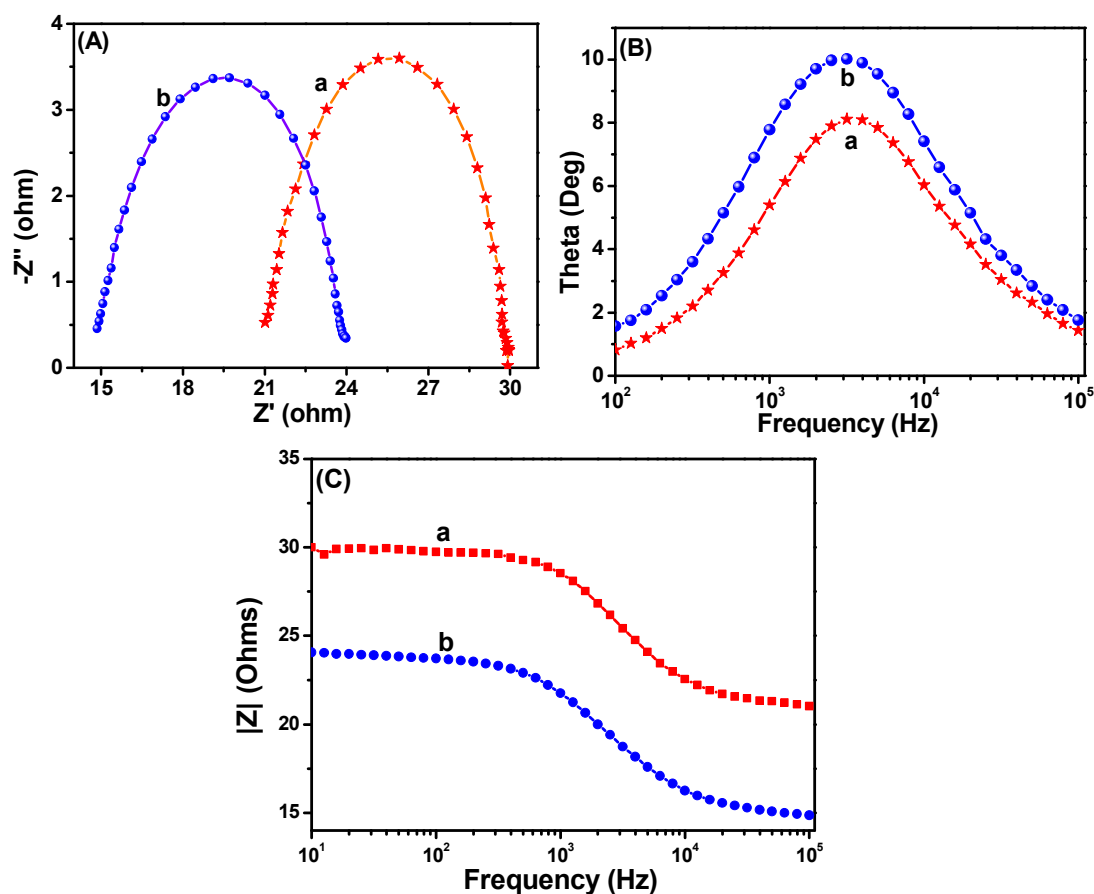


Fig. 9. (A) Nyquist plots, (B) Bode angle phase plots, and (C) Bode amplitude plots obtained for (a) TiO₂ and (b) Ag@TiO₂ nanocomposite (2.5 wt% of Ag content)-based DSSCs.

Furthermore, **Table 2** and **Fig. S3** summarize the results of the Nyquist plot. The Ag@TiO₂ exhibited a faster electron transport time ($\tau_s = R_s * C_\mu$)^{32, 34, 35} than the TiO₂. Hence its electron lifetime ($\tau_n = R_{ct} * C_\mu$)^{32, 34, 35} was significantly increased and survived from the recombination. The photovoltaic performance of the DSSC is clearly reflected by the charge collection efficiency (η_c)^{32, 34, 35} derived from $\eta_c = (1 + R_s/R_{ct})^{-1}$. Eventually, the charge collection efficiency was significantly increased with the addition of Ag. We can conclude that because of the longer τ_n and larger R_{ct} , the devices fabricated using Ag@TiO₂ showed improved J_{sc} values compared to TiO₂.

Table 2 Electrochemical parameters of TiO₂ and Ag@TiO₂ nanocomposite-based DSSCs.

Photoanode	R _s (Ω)	R _{ct} (Ω)	C _μ (μF)	τ _s (ms)	τ _n (ms)	η _c (%)
TiO ₂	21.13	8.77	7.22	0.15	0.06	29
Ag@TiO ₂	23.93	9.01	8.85	0.13	0.08	38

Footnote: The electrochemical impedance spectra (EIS) were recorded at an applied bias of -0.7 V in the frequency range of 0.01 Hz to 100 KHz. R_s: Device resistance; R_{ct}: Charge transfer resistance; C_μ: Chemical capacitance; τ_s: Electron transport time; τ_n: Electron lifetime; η_c: Charge collection efficiency.

3.7. Operation principle of Ag@TiO₂ plasmonic photoanode-based DSSC

The operation principle of the DSSC based on the Ag@TiO₂-modified photoelectrode under illumination is shown in **Fig. 10**. During light irradiation, the dye absorbs incident light and promotes electrons to the excited state. An excited electron is injected into the conduction band of the TiO₂ nanoparticles. The dye is then oxidized by receiving the electron

from the electrolyte through the redox system, and is ready to be used again. The electrolyte itself will regenerate via the platinum counter-electrode by an electron passing through the external circuit. In our study, the Ag deposited onto the TiO₂ surface not only acted as an electron sink for the photoinduced charge carriers but could also be used as a scattering element for plasmonic scattering to trap the light and near field coupled with the dye molecules.³⁶ This will eventually improve the optical absorption of the dye, resulting in a significant enhancement of the photocurrent (**Fig. 10**). Whenever the TiO₂ comes to contact with Ag, both will undergoes Fermi level equilibration to each other, resulted in the formation of Schottky barrier and thus led to large numbers of electron are accumulated at the surface of the metal (Ag) nanoparticles. This accumulation of electrons on the Ag nanoparticles shifted the position of the Fermi level closer to the conduction band of TiO₂.³⁷ The Schottky barrier formed between the Ag and TiO₂ helps to flow the electrons from the Ag to TiO₂ conduction band *via* rapid interfacial charge transfer process and were collected by the current collector (ITO), thus improve the photocurrent generation under irradiation.³⁸ Once the electrons being transfer to the conduction band of TiO₂, the photo-excited electrons from the dye, N719, will start to accumulate on Ag surface again. Furthermore, the formation of Schottky barrier at the Ag/TiO₂ interface, which could act as an electron sink, also will help to prevent the electron–hole recombination process.²⁴ The similar report also available for the metal-semiconductor (Ag-TiO₂) photoanode sensitized with N719 based DSSC.²¹

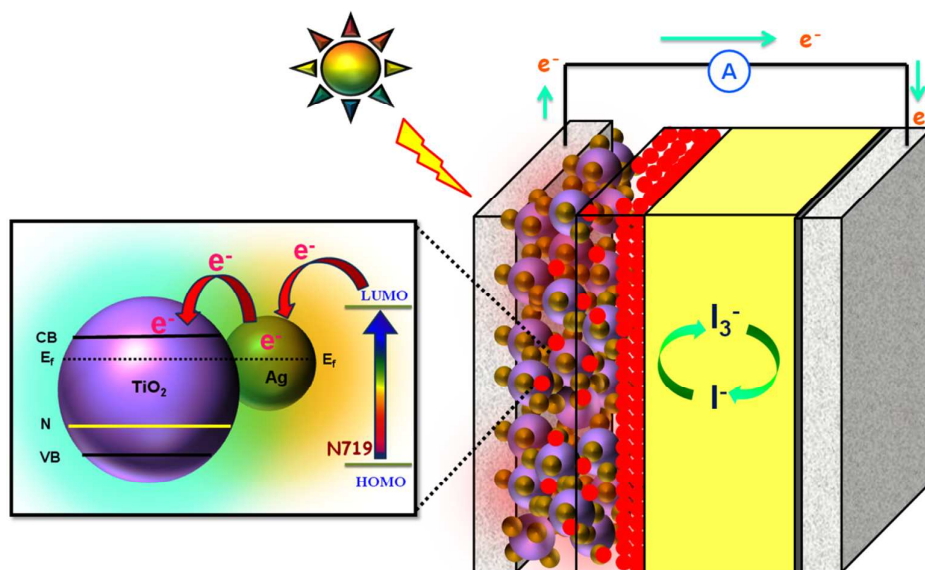


Fig. 10. Schematic functions of Ag@TiO₂ nanocomposite-modified photoanode-based dye-sensitized solar cells.

4. Conclusion

In conclusion, plasmonic silver nanoparticles modified titania (Ag@TiO₂) nanocomposite materials with various Ag contents were synthesized by simple chemical reduction method without using any stabilizer and surfactants. The as-prepared Ag@TiO₂ plasmonic nanocomposite materials were used as photoanode in the dye-sensitized solar cells to investigate the solar to electrical energy conversion ability. The incorporation of Ag on the TiO₂ surface significantly influenced the optical properties in the region of 400–500 nm because of the surface plasmon resonance effect and the formation of 2–4 nm sized Ag nanoparticles on the TiO₂ was confirmed through the HRTEM. The DSSC assembled with the Ag@TiO₂-plasmonic photoanode demonstrated an enhanced solar-to-electrical energy conversion efficiency (4.86 %) than that of bare TiO₂ (2.57 %) under an AM 1.5 G simulated solar irradiation of 100 mW cm⁻², due the surface plasmon resonance effect of Ag nanoparticles present in the nanocomposites. The influence of the Ag content on the overall efficiency was also investigated, and the optimized Ag content with TiO₂ was found to be 2.5

wt.%. The enhanced solar energy conversion efficiency of the Ag@TiO₂ plasmonic nanocomposite makes it a promising alternative to conventional photoanode-based DSSCs.

Acknowledgements

The authors wish to express their gratitude to the Ministry of Higher Education and the University of Malaya for sanctioning a High Impact Research Grant (UM.C/625/1/HIR/MOHE/SC/21) and UMRG Programme Grant (RP007C/13AFR). The authors also wish to thank the Synchrotron Light Research Institute, Nakhon Ratchasima, Thailand for the XPS measurements.

References

- 1 B. O'Regan and M. Gratzel, *Nature*, 1991, **353**, 737-740.
- 2 Q. Tao, X. Zhao, Y. Chen, J. Li, Q. Li, Y. Ma, J. Li, T. Cui, P. Zhu and X. Wang, *RSC Adv.*, 2013, **3**, 18317-18322.
- 3 H.-Y. Chen, D.-B. Kuang and C.-Y. Su, *J. Mater. Chem.*, 2012, **22**, 15475-15489.
- 4 J. van de Lagemaat, N. G. Park and A. J. Frank, *J. Phys. Chem.B*, 2000, **104**, 2044-2052.
- 5 N. Kopidakis, N. R. Neale, K. Zhu, J. van de Lagemaat and A. J. Frank, *Appl. Phys. Lett.*, 2005, **87**, 202106.
- 6 Y. Lai, H. Zhuang, K. Xie, D. Gong, Y. Tang, C. L. L. Sun and Z. Chen, *New J. Chem.*, 2010, 1335-1340.
- 7 J. M. Macak, F. Schmidt-Stein and P. Schmuki, *Electrochem. Commun.* 2007, **9**, 1783-1787.
- 8 L. Yang, D. He, Q. Cai and C. A. Grimes, *J. Phys. Chem. C*, 2007, **111**, 8214-8217.
- 9 H. Zhao, Y. Chen, X. Quan and X. Ruan, *Chin. Sci. Bull.*, 2007, **52**, 1456-1461.
- 10 D. M. Schaadt, B. Feng and E. T. Yu, *Appl. Phys. Lett.*, 2005, **86**, 063106.
- 11 C. F. Eagen, *Appl. Opt.*, 1981, **20**, 3035-3042.

- 12 J. J. Mock, M. Barbic, D. R. Smith, D. A. Schultz and S. Schultz, *J. Chem. Phys.*, 2002, **116**, 6755-6759.
- 13 G. Zhao, H. Kozuka and T. Yoko, *Sol. Energy Mater. Sol. Cells*, 1997, **46**, 219-231.
- 14 K.-C. Lee, S.-J. Lin, C.-H. Lin, C.-S. Tsai and Y.-J. Lu, *Surf. Coat. Technol.*, 2008, **202**, 5339-5342.
- 15 C. Wen, K. Ishikawa, M. Kishima and K. Yamada, *Sol. Energy Mater. Sol. Cells*, 2000, **61**, 339-351.
- 16 Y. Binyu, L. Kar Man, G. Qiuquan, L. Woon Ming and Y. Jun, *Nanotechnology*, 2011, **22**, 115603.
- 17 C.-S. Chou, R.-Y. Yang, C.-K. Yeh and Y.-J. Lin, *Powder Technol.*, 2009, **194**, 95-105.
- 18 J. Qi, X. Dang, P. T. Hammond and A. M. Belcher, *ACS Nano*, 2011, **5**, 7108-7116.
- 19 C. Photiphitak, P. Rakkwamsuk, P. Muthitamongkol, C. Sae-Kung and C. Thanachayanont, *Int. J. Photoenergy*, 2011, **2011**, 357979.
- 20 S. Chen, J. Li, K. Qian, W. Xu, Y. Lu, W. Huang and S. Yu, *Nano Res.*, 2010, **3**, 244-255.
- 21 Z. Tian, L. Wang, L. Jia, Q. Li, Q. Song, S. Su and H. Yang, *RSC Adv.*, 2013, **3**, 6369-6376.
- 22 A. Pandikumar, K. Sivaranjani, C. S. Gopinath and R. Ramaraj, *RSC Adv.*, 2013, **3**, 13390-13398.
- 23 S. P. Lim, N. M. Huang, H. N. Lim and M. Mazhar, *Int. J. Photoenergy* 2014, **2014**, 12.
- 24 J. Du, J. Zhang, Z. Liu, B. Han, T. Jiang and Y. Huang, *Langmuir* 2006, **22**, 1307-1312.
- 25 N. Chandrasekharan and P. V. Kamat, *J. Phys. Chem. B*, 2000, **104**, 10851-10857.
- 26 G. L. Chiarello, M. H. Aguirre and E. Selli, *J. Catal.*, 2010, **273**, 182-190.
- 27 K. Sivaranjani and C. S. Gopinath, *J. Mater. Chem.*, 2011, **21**, 2639-2647.
- 28 C. Su, L. Liu, M. Zhang, Y. Zhang and C. Shao, *CrystEngComm*, 2012, **14**, 3989-3999.
- 29 D. Briggs, *Surf. Interface Anal.*, 1981, **3**, 1.
- 30 L. Wang, L. Jia and Q. Li, *Mater. Lett.*, 2014, **123**, 83-86.

- 31 K. Guo, M. Li, X. Fang, X. Liu, B. Sebo, Y. Zhu, Z. Hu and X. Zhao, *J. Power Sources*, 2013, **230**, 155-160.
- 32 S. G. Kim, M. J. Ju, I. T. Choi, W. S. Choi, H.-J. Choi, J.-B. Baek and H. K. Kim, *RSC Adv.*, 2013, **3**, 16380-16386.
- 33 P. S. Archana, A. Gupta, M. M. Yusoff and R. Jose, *Phys. Chem. Chem. Phys.*, 2014, **16**, 7448-7454.
- 34 J. Nissfolk, K. Fredin, A. Hagfeldt and G. Boschloo, *J. Phys. Chem. B*, 2006, **110**, 17715-17718.
- 35 Q. Wang, Z. Zhang, S. M. Zakeeruddin and M. Grätzel, *J. Phys. Chem. C*, 2008, **112**, 7084-7092.
- 36 S. Lin, K. Lee, J. Wu and J. Wu, *Sol. Energy*, 2012, **86**, 2600-2605.
- 37 M. Ni, M. K. H. Leung, D. Y. C. Leung and K. Sumathy, *Renew. Sust. Energ. Rev.*, 2007, **11**, 401-425.
- 38 P. Christopher, D. B. Ingram and S. Linic, *J. Phys. Chem. C*, 2010, **114**, 9173-9177.